Cellular diversity and genetic alterations in light chain amyloidosis and amyloidosis with co-occurring multiple myeloma

Ankita Srivastava[1*], Romika Kumari[1*], Juho J. Miettinen[1], Minna H. Suvela[1], Klara Acs[2], Sini Luoma[3], Caroline A. Heckman[1]

[1]Institute for Molecular Medicine Finland - FIMM, HiLIFE – Helsinki Institute of Life Science, iCAN Digital Precision Cancer Medicine Flagship, University of Helsinki, Helsinki, Finland;
[2]Oncopeptides AB, Stockholm, Sweden;
[3]Department of Hematology, Comprehensive Cancer Center, Helsinki University Hospital and University of Helsinki, Helsinki, Finland
*These authors contributed equally

Corresponding author: Dr. Caroline A. Heckman, Institute for Molecular Medicine Finland - FIMM, University of Helsinki, P.O. Box 20 (Tukholmankatu 8), 00014 University of Helsinki, Finland; Email address: caroline.heckman@helsinki.fi

KEY POINTS

1. 1q gain is mainly restricted to amyloidosis patients with co-occurring sMM, MM, or MGUS.
2. Multiple genes located on chromosome 1 are upregulated in plasma cells of patients with co-occurring AL and MM, potentially contributing to disease progression.

ABSTRACT

Immunoglobulin light-chain amyloidosis (AL) has been reported to be associated with multiple myeloma (MM) in approximately 10-15% of cases, with the two conditions often coexisting. Understanding the interaction between these diseases is vital for improving patient outcome and developing targeted treatments. Our study investigates cellular heterogeneity in immunoglobulin light-chain amyloidosis (AL) and coexisting multiple myeloma (MM) or monoclonal gammopathy of undetermined significance (MGUS) (AL_MM) using single-cell RNA sequencing (scRNA-seq). A total of 21 bone marrow samples from 20 patients were analyzed, including 9 with AL_MM.

We observed exclusive association of the 1q gain chromosomal aberration with the AL_MM group ($p<0.01$). The scRNA-seq data revealed 27 distinct cell clusters representing 14 unique cell types, with 6 clusters identified as plasma cell (PC) subpopulations. These subpopulations exhibited considerable inter- and intra-individual heterogeneity.

Comparative analysis between the AL and AL_MM groups showed higher proportions of GMP, HSC, cDC2, and T cells in the AL group ($p<0.05$), suggesting a distinct tumor microenvironment. Differential gene expression analysis between the two groups identified 152 up-regulated and 134 down-regulated genes in AL_MM samples, with 28 of the up-regulated genes and 1 downregulated gene located on chromosome 1q. Furthermore, the application of inferCNV to the scRNA-seq data revealed amplifications in chromosome 4, 7, 11, 20, and 22 of AL samples.

Our findings enhance the understanding of the molecular mechanisms underlying AL and its progression in patients with coexisting MM or MGUS. The study provides valuable insights into disease progression and cellular variability, supporting improved patient stratification and the development of targeted therapies for these complex hematological conditions.

INTRODUCTION

Light-chain amyloidosis (AL) is a plasma cell disorder characterized by the secretion of unstable amyloidogenic immunoglobulin light chains that assemble as amyloid fibrils[1]. These amyloid deposits infiltrate various tissues, disrupting their normal function. The kidneys, heart, gastrointestinal tract, liver and autonomous nervous system are some of the most frequently affected organs by the extracellular amyloid deposition[2]. In contrast, multiple myeloma (MM) results from the clonal proliferation of the malignant plasma cells, which produces monoclonal immunoglobulins[3]. Both MM and AL are clonal plasma cell disorders, but the co-occurrence of two monoclonal gammopathies is a rare event. Notably, approximately 10-15% of AL cases are reported to be associated with MM[4]. AL can be established in newly diagnosed patients with MM[5] or can emerge later during the course of disease6. The molecular mechanism underlying the association between AL and MM remains unclear. Increased levels of bone marrow plasma cells in patients with AL have been previously associated with poor overall survival[6]. Patients with concurrent AL and MM are often

excluded from clinical trials and tend to have poor prognosis and reduced overall survival[7,8]. Given that the approved standard of care is different for AL and MM, further investigation into the coexistence of these conditions is essential to enhance treatment strategies and to better understand the prognostic implications and characteristics of this association.

In this study, we employed single-cell RNA sequencing (scRNA-seq) to accurately assess the variability and heterogeneity at the cellular level in patients diagnosed with isolated light chain AL and AL with co-occurring multiple myeloma or monoclonal gammopathy of undetermined significance (MGUS) (collectively referred to as AL_MM in this study). We also explored large-scale somatic chromosomal copy number alterations in these samples using inferCNV[9]. Additionally, we analyzed the clinical data from the associated patient samples to identify distinguishing factors between patients with isolated AL and patients with AL and co-occurring MM/MGUS.

METHODS

Sample collection

The Finnish Hematology Registry and Biobank provided 21 samples of viable frozen bone marrow mononuclear cells (BM-MNCs) from 20 patients diagnosed with AL, with all samples collected at the time of diagnosis (n=20) and one patient providing an additional sample at relapse (n=1). Among these samples, 9 were from patients with co-occurring diseases including multiple myeloma (MM) (n=3), smoldering multiple myeloma (sMM) (n=5), or monoclonal gammopathy of undetermined significance (MGUS) (n=1), collectively referred to as the AL_MM group in this study. The associated clinical data included cytogenetic information obtained through fluorescent in situ hybridization (FISH). Samples were collected following informed consent and in accordance with protocols approved by the ethical committee of the Helsinki University Hospital Comprehensive Cancer Center (permit numbers 239/13/03/00/2010, 303/13/03/01/2011), and in compliance with the Declaration of Helsinki (**Figure 1A**).

Single cell RNA-sequencing

Using fluorescence-activated cell sorting, viable frozen BM-MNCs were thawed and sorted based on cell viability using 7AAD and the expression of the plasma cell marker CD138 (APC labeled clone MI15 antibody from BD Biosciences, Santa Clara, CA). Single-cell RNA sequencing was performed using the Chromium Single Cell 3' Gene

Expression v3 reagent kit (10x Genomics, Pleasanton, CA). The manufacturer's instructions were followed for generating gel beads in emulsion (GEM), cDNA amplification, and library preparation. Between 4,000 and 9,000 live CD138- cells, along with varying amounts of CD138+ cells, were loaded per Chromium chip lane. All sorted CD138+ cells were included for sequencing; however, the concentration of these cells was not measured due to the low number of CD138+ cells. Sequencing of the prepared libraries was performed using the Illumina NovaSeq 6000 system, which provided paired end reads of 28 bp and 89 bp.

Data processing and analysis

The 10x Genomics Cell Ranger v6.0.2 pipelines were used for data processing and analysis. Specifically, 'cellranger mkfastq' was used to produce FASTQ raw sequence data files and 'cellranger count' was used to perform alignments, filtering and UMI (unique molecular identifier) counting. The alignments were performed against human genome GRCh38[10].

Further, the output generated by the cellranger pipeline was used as input for the Seurat (version 5.1.0) tool[11]. Using Seurat, data quality control was performed, and the cells were selected for further analysis. Cells exhibiting low quality/dying cells and cell doublets or multiplets were filtered out using the filters nFeature_RNA > 200 and percent.mt cutoff was < triple median or 20%, whichever was the smaller value. After removing the unwanted cells, the data was normalized using the 'LogNormalize' method. Next, the top 2000 highly variable features were selected for downstream analysis. The batch effect in the data was corrected using the 'rpca' method. For linear dimension reduction, PCA was performed on the scaled data and the first 20 PCs were used in the 'FindNeighbors' function. A resolution of 0.8 and Louvain algorithm was used in 'Findclusters' function for clustering the cells. A non-linear dimensional reduction technique UMAP was used for visualization of the datasets. Differentially expressed genes were identified for all the clusters using 'FindAllMarkers' function with min.pct=0.25 and logfc.threshold=0.25. To assign cell type identity to the clusters, we used Azimuth[12], and mononuclear cell markers were obtained from sctype database[13]. Further, to recognize the heterogeneity and similarities among the various cell populations, we investigated the enriched biological processes within these cell types using Escape v2.1.0[14]. To perform differential expression analysis within plasma cells from AL and AL_MM samples, we employed single-cell and pseudobulk DE

testing from the Seurat tool. The genes which were consistently significant (p_val.bulk <0.05; p_val.sc <0.05) in both methods were identified as differentially expressed (DE) genes. Comparative pathway analysis between AL and AL_MM samples was done using 'Single cell pathway analysis' (SCPA)[15] and was further validated with fGSEA (fast preranked gene set enrichment analysis)[16]. For the identification of drug-gene interaction of DE genes we used DGIdb (v5.0)[17].

To predict gene interaction networks, we used 'The search tool for the retrieval of interacting genes/proteins (STRING)'[18]. To identify somatic large-scale chromosomal copy number alterations including gains and deletions of entire chromosome or large segments of the chromosomes, we used InferCNV[9]. For inferCNV, we used the following cell types: CD8 effector, natural killer cells, CD14 monocytes, CD4 memory, CD16 monocytes, late erythroid, hematopoietic stem cells (HSC), granulocyte monocyte progenitors (GMP) , plasmacytoid dendritic cells (pDC), conventional dendritic cells 2 (cDC2) and T cells as the normal cell types (non-tumor) and precursor B cells (Pro B) , B cells and plasma cell as malignant cell types. The parameters we used included cutoff=0.1, cluster_by_groups=T, denoise=T and HMM=T. Further, we utilized the output from the inferCNV analysis, particularly the expression data matrix found in the expr.data slot of the inferCNV object (infercnv_obj@expr.data), to combine the inferCNV results from 21 samples. The expression data matrix contains the processed and normalized gene expression values for all cells in each sample. Each gene in the matrix was mapped with its specific cytoband based on its location in the genome. For each sample, we followed these steps; a) we grouped genes according to their cytobands; b) we calculated the average expression value for all genes within each cytoband. The student's t-test was used to identify significant differences (p-value<0.05) in chromosomal copy number alterations between the AL and AL_MM groups.

RESULTS

Exclusive 1q gain in AL with co-occurring MM

To thoroughly examine the differences between patients diagnosed solely with light chain amyloidosis (AL) and those with co-occurring multiple myeloma/MGUS (AL_MM) we analyzed clinical data from 21 patient samples (diagnosis: n=20; relapse: n=1). Our patient cohort included 13 male and 8 female participants, with a median age of 66 years and median survival time of 46.5 months. The samples comprised

both lambda and kappa light chain amyloidosis (lambda: n=14; kappa: n=2; missing: n=5) and exhibited various cytogenetic aberrations, with 1q gain (6/21), t(11;14)(5/21) and trisomy 11(5/21) being the most frequent abnormalities (**Table 1**), in line with previous reports[19].

Further clinical data indicated that 12 patients were diagnosed with only amyloidosis (AL), while 9 patients had co-occurring diseases including multiple myeloma (MM)(n=3), smoldering multiple myeloma (sMM)(n=5), or monoclonal gammopathy of undetermined significance (MGUS) (n=1), and collectively referred to as the AL_MM group. We did not find a significant difference in the overall survival of these two sub-groups (AL and AL_MM). However, a comparison of the cytogenetic aberrations associated with these groups showed that the chromosome 1q gain was exclusive to the patients of AL_MM group (Chi-squared test $p<0.01$) (**Figure1B**). Other cytogenetic aberrations, such as t(11;14), monosomy 13, trisomy 11 were more frequently observed in AL group, but no significant difference was noted ($p>0.05$) in the frequencies between the two groups.

The immune microenvironment in AL

We successfully sequenced a total of 151,164 cells with an average of 8,679 reads and a median of 756 genes expressed per cell. From the integrated data of 21 samples analyzed using the Seurat tool, we identified 27 cell clusters representing 14 distinct cell-type populations based on their transcriptome profiles (**Figure 1C and D**). These clusters were annotated according to the expression of the known cell type biomarkers, as shown in **Supplemental Figure 1** (see the methods section for additional details). The identified cell types included plasma cells, natural killer (NK) cells, CD8 effector cells, CD14 and CD16 monocytes, CD4 memory, T cells, late erythrocytes, B cells, Pro B, granulocyte monocyte progenitor (GMP), hematopoietic stem cells (HSC), conventional (cDC2) and plasmacytoid dendritic cells (pDC) (**Figure 1C-D**). The cell types that exhibited more than one cluster included plasma cells (n=6), late erythrocytes (n=3), CD14 monocytes (n=2), CD4 memory cells (n=2), natural killer cells (n=3) and CD8 effectors cells (n=3). This clustering of the same cell-type in more than one cluster can be attributed to factors like cell states and biological heterogeneity[20].

Further, plasma cells were the most abundant cell type among the obtained clusters constituting 29.62% of the total cells, as expected given that CD138+ cell enrichment

was performed prior to sequencing followed by CD8 effector cells (21.63%), NK cells (16.29%), CD14 monocyte cells (10.42%) (**Figure 1C**).

To further investigate the tumor micro-environment in AL, we examined the correlation between the proportion of different predicted cell types. We found that the proportions of most of other cell types were negatively correlated with the proportions of plasma cells, including CD4 memory T cells (r=-0.57; p=0.0078), CD14 monocytes (r=-0.49; p=0.025) and CD16 monocytes (r=-0.41; p=0.07) (**Supplemental Figure 2A-B**), which can be attributed by the disruption of the normal hematopoiesis by the excessively proliferating plasma cells[4]. Lymphocytes (including T cells, NK cells, CD4 memory, CD8 effector, B cells, pro B and plasma cells) and myeloid cells (including CD16 monocytes, CD14 monocytes, late erythroid, GMP, HSC, pDC and cDC2 cells) were clearly distinguishable based on the enriched biological states identified using Escape v2.1.0[14]. One of these biological processes was the 'KRAS_SIGNALING_DN' gene set, which includes genes that are downregulated by 'KRAS activation', and this gene set was significantly enriched in the lymphocytes (**Supplemental Figure 2C, D-E**).

Clonal diversity of plasma cell in AL and AL with co-occurring MM

A total of 6 plasma cell clusters were identified from the aggregated cells (n= 30,172 plasma cells out of 101,831 total cells) derived from 21 patient samples. These clusters were annotated based on the plasma cell markers presented in **Supplemental Figure 1.** The clustering of the plasma cells according to their gene expression profiles revealed significant heterogeneity at the inter and intra individual level, with plasma cells categorized into clusters PC_01, PC_02, PC_03, PC_04, PC_05 and PC_06 indicating distinct transcriptome profiles (**Figure 2A**). Furthermore, these plasma cell clusters were uniformly distributed across different samples, highlighting the tumor heterogeneity and clonal evolution within all samples (**Figure 2B**). The overall proportions of the plasma cells were higher in the AL_MM samples, but the difference was not statistically significant (**Supplementary Figure 3**). Analysis of gene expression within these clusters revealed up-regulation of various gene sets, including immunoglobulin genes (**Figure 2C**). Additionally, pathway enrichment analysis indicated that PC_01 and PC_06 shared similar pathways, while PC_02 and PC_03 were more comparable to each other. In contrast, PC_04 and PC_05 had the most distinct transcriptional profiles and showed the least similarity to other plasma cell clusters (**Figure 2D**).

Cellular and transcriptomic changes from diagnosis to relapse stage

The samples from patient AL_MM_P15 were collected at both the diagnosis and relapse stages. A comparison of the cell-type proportions between these stages revealed an increase in plasma cells (1.7%), indicating a higher tumor burden at relapse. Additionally, we observed an increase in the proportions of CD4 memory cells (12.9%), CD16 monocytes (4.5%), late erythrocytes (3.5%), GMP (0.4%), HSC (0.3%), pDC (0.1%), cDC2 (0.3%), and T cells (0.3%). Conversely, the proportions of NK cells (5.1%), CD8 effector (13.6%), CD14 monocytes (0.8%), B cells (3.9%), and pro B cells (0.6%) were found to be lower at relapse (**Figure 3A**). Also, we observed a certain degree of heterogeneity within the transcriptome profiles of the plasma cell populations between diagnosis and relapse, indicating tumor clonal evolution from diagnosis to relapse (**Figure 3B**). Differential gene expression analysis of plasma cells from the paired samples identified 21 genes with altered regulation. The diagnosis sample showed upregulation of the following genes: *IFI44L, S100A9, XAF1, MX1, GIMAP7, IFI44, IFI6, GIMAP4, CX3CR1, CHST2, HERC6, IL1B, AIF1, and EPSTI1*. Meanwhile, the genes *IGLC2, IGHD, PER1, ENC1, U2AF1, GRASP, and IGLV3-1* were downregulated **(Figure 3C).** Given that the paired sample size in this study was limited to just one pair, these findings should be interpreted with caution and should be further validated in a larger cohort.

Higher myeloid and T-cell proportions in the AL group

The samples were divided into two distinct groups based on their diagnosis: the AL group (n=12) which includes samples diagnosed solely with amyloidosis, and the AL_MM group (n=9) which consists of samples from patients with co-occurring smoldering multiple myeloma (n=5), multiple myeloma (n=3) or monoclonal gammopathy of undetermined significance (MGUS)(n=1). To explore the similarities and differences between AL and AL_MM at the single cell level, we conducted a comparative analysis. This analysis revealed significantly higher proportions of GMP (p=0.0043), HSC (p=0.0043), cDC2 (p=0.0033) and T cells (p=0.049) in the AL group (**Figure 3D**). Although the plasma cell proportion was higher in the AL_MM samples, this difference was not statistically significant (**Supplementary Figure 3**). Analysis of individual plasma cell clusters showed that all clusters were present in both the AL as

well as the AL_MM group, with all plasma cell clusters being relatively more abundant in the AL_MM group (**Figure 3E**).

Distinct plasma cell profiles in AL and AL with co-occurring MM

Differential expression analysis of plasma cells from AL and AL_MM sub-groups identified 152 genes as upregulated and 134 genes as down-regulated (**Supplemental Figure 4A-B**). Gene-gene interaction networks were analyzed and visually represented using the STRING database[18] for both upregulated and downregulated genes. For upregulated genes in AL_MM, the analysis showed a highly significant enrichment (p = 2.18e-14) of gene interactions among 139 genes, particularly in RNA-related processes and ribosomal functions. The network revealed higher connectivity, with enriched GO terms including gene expression, RNA metabolic processes, and ribonucleoprotein complex biogenesis, suggesting altered RNA metabolism and protein synthesis mechanisms may play a role in AL_MM pathology. Similarly, for downregulated genes, the analysis revealed a highly significant enrichment (p = 2.42e-07) of gene interactions among the 119 genes, mostly in extracellular and vesicle-related processes, with significant GO terms being extracellular exosome, vesicle, and endoplasmic reticulum membrane. These findings suggest that altered vesicular trafficking and protein secretion mechanisms may play a role in AL samples pathology (**Supplemental Figure 4C-D**). As mentioned earlier, utilizing cytogenetics data, we found that chromosome 1q gain was exclusively associated with the AL_MM samples (**Figure 1B**). Additionally, in the differential expression analysis, we observed that 29/152 upregulated genes in AL_MM were located on the long arm of chromosome 1 (1q) (**Figure 4A**). Overall, the expression profiles of the genes on 1q showed a marked upregulation in the AL_MM samples, except tumor suppressor gene *G0S2*[21] (**Figure 4B**).

Relative pathway enrichment analysis of the plasma cell populations in the AL and AL_MM samples revealed significant differences in the multivariate distributions of several key pathways. The top five pathways which showed notable changes included apoptosis, (p_{adj} = 2.78e-58, Qval = 7.59, fold change (FC) = -10.34), TNF signaling via NFkB (p_{adj} = 1.55e-54, Qval = 7.34, FC = -17.41), the p53 pathway (p_{adj} = 6.07e-43, Qval= 6.50, FC = -8.03), IL2 STAT5 signaling (p_{adj} = 1.08e-38, Qval = 6.16, FC = -10.74), and MYC targets V1 (p_{adj} = 1.08e-38, Qval = 6.16, FC = -6.25). These findings

indicate distinct gene expression patterns of plasma cells from patients with AL and those from patients with AL_MM (SCPA p_{adj} <0.05) (**Figure 4C**). Further, we used fast gene set enrichment analysis (fgsea) to investigate pathway enrichment patterns (up or down regulated)[41], the only significantly (p_{adj} = 0.0087) positively enriched pathway was '*KRAS signaling down*' with a normalized enrichment score (NES) of 2.266, indicating significant upregulation in AL_MM samples. Conversely, the most negatively enriched pathway was oxidative phosphorylation with an NES of -8.356 and an adjusted p-value of 0.0050, highlighting substantial downregulation. Additional pathways including MYC targets V1 (NES: -6.559), apoptosis (NES: -4.199), TNF signaling via NF-κB (NES: -4.107), and IL2/STAT5 signaling (NES: -3.028) were also significantly negatively enriched (all p_{adj} =0.0050), consistent with SCPA results. (**Supplementary Figure 5)**.

Drug-gene interactions highlight therapeutic candidates

To identify the druggable therapeutic targets in our differentially regulated genes we performed drug-gene interaction analysis which revealed that, out of 152 upregulated genes, 17 genes were categorized under the druggable genome category, 15 as enzymes, 8 as clinically actionable, 5 as tumor suppressors, 4 as DNA repair and 2 as cell surface genes. Further, 27 genes were found to interact with approved agents, key genes like *BAX*, *POLR1G*, and *NR3C1* showed interactions with approved drugs such as melphalan, and corticosteroids, which are commonly used in MM treatment regimens and cisplatin, which is used in treatment of several cancer types. Similarly, among the 134 downregulated genes, 40 genes were classified into the druggable genome category, 22 as enzymes, 11 as clinically actionable, 8 as cell surface genes, 4 as protease inhibitors, 2 genes in the protease category and 1 as a tumor suppressor. Also, 26 genes were found to have interactions with approved agents, including genes *ATF5*, *NCOA3*, and *NT5E* which showed interactions with antineoplastic agents such as vincristine, etoposide, and doxorubicin. These findings highlight candidate genes that could be explored for their potential as druggable targets in light chain amyloidosis along or with co-occurring multiple myeloma (**Supplementary Table 1**).

InferCNV uncovers distinct genomic alterations in AL and AL with co-occurring MM

Somatic large-scale chromosomal copy number alterations, including gains and deletion of large segments of chromosomes, were identified using inferCNV[9], where plasma cells, B cells and pro B cells were considered as malignant cell populations and all other cell types were used as reference (non-tumor) for comparison. In plasma cells, significant amplifications were observed in large segments of chromosomes 4 (4q21.21, 4q21.3 and 4q22.3), 7 (7q31.32, 7q31.33, 7q32.1, 7q32.2, 7q32.3 and 7q33), 11 (11q13.1, 11q13.2 and 11q13.3), 20 (20q11.22, 20q11.23, 20q12, 20q13.11 and 20q13.12) and 22 (22q11.22, 22q11.23 and 22q13.33) in the AL patient samples ($p<0.05$) (**Figure 5A-B**). Additionally, smaller segments of chromosomes 3 (3p21.2 and 3p21.1), 13 (13q14.2) and 19 (19q13.31) were also amplified ($p<0.05$). Furthermore, we found that chromosomes 2 (2q14.1 and 2q14.2), 17 (17q12 and 17q21.1) and 18 (18q22.2) were amplified in the AL_MM patient samples ($p<0.05$) (**Supplementary Figure 6A**). The B cells and pro B cells also exhibited some copy number alterations (**Supplementary Figure 6B**). Additionally, the inferCNV output for individual samples which had a sufficient number of plasma cells, highlighted the gain of chromosome 1q in some proportion of plasma cells including, AL_MM_P08, AL_MM_P10, AL_MM_P14, these findings were consistent with the FISH findings. We have included the inferCNV output for each sample in **Supplementary Figure 7**.

DISCUSSION

Few studies have described the co-existence of AL and MM [8,22-24].Patients with isolated AL amyloidosis typically exhibit lower bone marrow plasma cell infiltration and more frequent cardiac involvement. In contrast, those with concurrent AL amyloidosis and MM show a higher plasma cell burden, increased bone disease, and a poorer prognosis, with cardiac involvement being a key determinant of survival. These findings underscore the clinical importance of distinguishing between the two conditions and highlight the need for further research into their cellular and molecular differences. Further, individuals diagnosed with co-occurring AL and MM are frequently excluded from clinical trials and generally exhibit decreased overall survival[7,8]. Currently there are no established treatment guidelines for this complex patient population. By elucidating the pathogenetic mechanisms underlying the rare co-existence of these two diseases, our study contributes to the development of more effective treatment strategies for these patients.

In our patient cohort we reported that 9/21 (42.86%) patient samples diagnosed with AL had a coexisting sMM/MM or MGUS (AL_MM). Additionally, the cytogenetics analysis uncovered that chromosome 1q gain was exclusively associated with the AL_MM patients ($p<0.01$). 1q gain has previously been associated with the AL progression to MM and more aggressive forms of disease with poor overall survival[25]. This finding warrants further investigation to assess the potential of 1q gain as a prognostic marker for AL progression to MM. Other cytogenetic abnormalities, such as t(11;14) (25%), monosomy 13 (20%) and trisomy 11 (20%), were more common in the AL group, though the differences were not statistically significant, which may be attributable to the small cohort size. The association of t(11;14) with AL has been reported in a larger cohort by He et al., 2023[22], where the presence of t(11;14) was found to be associated with shorter median overall survival (OS) and progression free survival (PFS).

Single cell RNA sequencing analysis provided a comprehensive landscape of the cellular diversity in AL and AL_MM patients, with identification of 27 clusters spanning 14 different cell types. Besides plasma cells, the most abundant cell types were CD8 effector cells (21.63%) and natural killer cells (16.29%). The enrichment of CD8+ T cells in AL has been reported previously by Szalat et al., 2023[26]. The correlation analysis further indicated a negative relationship between plasma cells and other immune cell types, such as CD4 memory T cells and CD14 and CD16 monocytes. This suggests an immunosuppressive microenvironment which may contribute to tumor evasion from immune surveillance[27,28].

A notable finding of this study is the significant heterogeneity observed in plasma cell populations, with six distinct clusters identified (PC_01 to PC_06). This heterogeneity suggests ongoing clonal evolution within individual patients, even in cases of concurrent amyloidosis and multiple myeloma. The varying transcriptomic profiles of plasma cells across clusters could represent different stages of disease evolution. High inter-individual variability in plasma cells of AL has been previously reported by Wang et al., 2021[29]. Significant heterogeneity and sub-clonal evolution among plasma cells from longitudinal samples at different disease stages of MM detected by scRNA-seq has been described earlier[30]. In our study, the plasma cell heterogeneity and sub-clonal evolution was further supported by pathway enrichment analysis which revealed that some plasma cell clusters share similar pathway enrichments, whereas others

were more distinct. This divergence in pathway activation between clusters may indicate varying levels of malignancy within the plasma cell subpopulations.

It has been reported that HSCs and GMPs are significantly diminished in the bone marrow of MM patients compared to healthy donors[31]. Also, the higher levels of HSCs and lower levels of NK and CD4+ cells have been associated with AL in comparison to MGUS, sMM and MM[26]. From our analysis, we observed lower proportions of GMPs, HSCs, cDC2, and T cells in the AL_MM group. We also noticed higher plasma cell proportions in the AL_MM group compared to amyloidosis alone, whereas the difference was not statistically significant. Significantly higher proportions of plasma cells in amyloidosis with co-occurring multiple myeloma have been reported earlier in a large study of 1,255 patients[4].

Differential gene expression analysis of the PCs from the AL and AL_MM groups revealed upregulation of several genes located on chromosome 1 in the AL_MM group. Among these genes, *HDGF* has been reported to influence MM cell viability and alter the tumor microenvironment[32], *ATP1B1* is linked to adverse prognosis in various cancers[33], while *SMYD3* has been implicated in cancer development and progression[34]. Additionally, *CCT3* is associated with poor prognosis in MM[35], and *C1orf35* promotes tumorigenesis by activating c-MYC transcription in MM[36]. *ACBD6* shows significant upregulation in MM[37], and *DAP3* acts as a potent oncogenic protein across multiple cancer types[38]. Furthermore, *PSMD4* is identified as a novel target gene correlated with 1q21 amplification in patients with sMM and MM[39], while increased expression of *SETDB1* is linked to poor progression in MM[40]. Lastly, *ADAM15* plays a role in MM progression and proliferation signaling[41]. This suggests that up-regulation of these genes may be significant in the development and progression of multiple myeloma in patients with amyloidosis.

We also explored the druggable targets among the differentially expressed genes where 27 up-regulated and 26 down-regulated genes were found to interact with the approved agents. One of the most prominently connected genes was BAX, a pro-apoptotic regulator and it exhibited interactions with over 40 approved compounds including chemotherapeutics such as cisplatin, docetaxel, vinorelbine, etoposide and methotrexate, as well as glucocorticoids and hormonal agents. A recent report highlighted that MM with 1q gain may be more sensitive to MCL1 and PI3K inhibitors[42], It has also been reported that dual targeting of BAX and MCL1 synergistically induces apoptosis in cells resistant to MCL1 inhibitor as a single agent therapy[43]. Our findings

show that BAX could be explored for its potential as druggable targets in AL_MM. Also, expression of *PSMD4*, which is known to be elevated in MM with the 1q gain and is also associated with the poor overall survival was reported in our study to exhibit interactions with multiple proteasome inhibitors (PI) including bortezomib and carfilzomib. Targeting PSMD4 has been explored as a therapeutic strategy in proteasome inhibitor resistant MM[44] and should be explored further in AL_MM.

Using inferCNV, we were able to identify large-scale somatic chromosomal copy number alterations, including both gains and deletions[9] in both AL and AL_MM samples that were not detected by clinical cytogenetic analysis. Specifically, AL samples showed amplifications on chromosomes 4, 7, 11, 20, and 22, while AL_MM samples displayed amplifications on chromosomes 2, 17, and 18. Traditionally, interphase fluorescence in situ hybridization (iFISH) has been used to predict copy number alterations, but FISH studies are limited to probing individual chromosomes[45]. In contrast, inferCNV enables the detection of sub-chromosomal copy number alterations (CNAs) across all chromosomes in every sample. In our first scRNA-seq-based CNV prediction analysis for amyloidosis samples, we uncovered novel aberrations that warrant further investigation.

This study, while providing valuable insights into the co-occurrence of amyloidosis and multiple myeloma, however its small sample size limits the statistical power of the findings, which should be validated in a larger cohort. In conclusion, our findings pave the way for further investigations into the distinct and overlapping molecular mechanisms characterizing these diseases and which could potentially inform for more personalized treatment strategies in the future.

ACKNOWLEDGEMENTS

The authors are grateful for the generous donation of samples from the contributing patients. The samples were obtained from the Finnish Hematology Registry and Biobank. The authors also thank the FIMM Single-Cell Analytics and Genomics Units, which are supported by HiLIFE and Biocenter Finland. This work has been supported by funding from Oncopeptides. We acknowledge the use of ChatGPT for text formatting and language polishing. The authors also acknowledge the use of BioRender.com for the generation of figure illustrations.

AUTHORSHIP CONTRIBUTIONS

CAH, AS, and RK contributed to the conception/design of the study with support from KA. Data analysis was performed by AS with advice from RK and CAH. RK wrote the manuscript with support from AS and CAH. JJM and MHS contributed to single cell sequencing sample preparation. SL provided clinical data related to the samples. All authors critically reviewed and contributed to the final manuscript.

DISCLOSURE OF CONFLICTS OF INTEREST

All authors met the criteria set forth by the International Committee of Medical Journal Editors (ICMJE) and hence adequately contributed to manuscript development. KA was an employee for Oncopeptides AB. CAH has received research funding from Oncopeptides to support this study. CAH has received funding from Kronos Bio, Novartis, Celgene, Orion Pharma and the IMI2 consortium project HARMONY unrelated to this work.

REFERENCES

1. Merlini G, Stone MJ. Dangerous small B-cell clones. *Blood*. 2006;108(8):2520-2530.
2. Obici L, Perfetti V, Palladini G, Moratti R, Merlini G. Clinical aspects of systemic amyloid diseases. *Biochim Biophys Acta*. 2005;1753(1):11-22.
3. van de Donk N, Pawlyn C, Yong KL. Multiple myeloma. *Lancet*. 2021;397(10272):410-427.
4. Kourelis TV, Kumar SK, Gertz MA, et al. Coexistent multiple myeloma or increased bone marrow plasma cells define equally high-risk populations in patients with immunoglobulin light chain amyloidosis. *J Clin Oncol*. 2013;31(34):4319-4324.
5. Siragusa S, Morice W, Gertz MA, et al. Asymptomatic immunoglobulin light chain amyloidosis (AL) at the time of diagnostic bone marrow biopsy in newly diagnosed patients with multiple myeloma and smoldering myeloma. A series of 144 cases and a review of the literature. *Ann Hematol*. 2011;90(1):101-106.
6. Paiva B, Vidriales MB, Perez JJ, et al. The clinical utility and prognostic value of multiparameter flow cytometry immunophenotyping in light-chain amyloidosis. *Blood*. 2011;117(13):3613-3616.
7. Bahlis NJ, Lazarus HM. Multiple myeloma-associated AL amyloidosis: is a distinctive therapeutic approach warranted? *Bone Marrow Transplant*. 2006;38(1):7-15.
8. Rios-Tamayo R, Krsnik I, Gomez-Bueno M, et al. AL Amyloidosis and Multiple Myeloma: A Complex Scenario in Which Cardiac Involvement Remains the Key Prognostic Factor. *Life (Basel)*. 2023;13(7).
9. Tickle T TI, Georgescu C, Brown M, Haas B. inferCNV of the Trinity CTAT Project.. Klarman Cell Observatory, Broad Institute of MIT and Harvard, Cambridge, MA, USA. https://github.com/broadinstitute/inferCNV.; 2019.
10. Schneider VA, Graves-Lindsay T, Howe K, et al. Evaluation of GRCh38 and de novo haploid genome assemblies demonstrates the enduring quality of the reference assembly. *Genome Res*. 2017;27(5):849-864.

11. Stuart T, Butler A, Hoffman P, et al. Comprehensive Integration of Single-Cell Data. *Cell*. 2019;177(7):1888-1902 e1821.
12. Hao Y, Hao S, Andersen-Nissen E, et al. Integrated analysis of multimodal single-cell data. *Cell*. 2021;184(13):3573-3587 e3529.
13. Ianevski A, Giri AK, Aittokallio T. Fully-automated and ultra-fast cell-type identification using specific marker combinations from single-cell transcriptomic data. *Nat Commun*. 2022;13(1):1246.
14. Borcherding N, Vishwakarma A, Voigt AP, et al. Mapping the immune environment in clear cell renal carcinoma by single-cell genomics. *Commun Biol*. 2021;4(1):122.
15. Bibby JA, Agarwal D, Freiwald T, et al. Systematic single-cell pathway analysis to characterize early T cell activation. *Cell Rep*. 2022;41(8):111697.
16. Korotkevich G, Sukhov V, Budin N, Shpak B, Artyomov MN, Sergushichev A. Fast gene set enrichment analysis. 2021.
17. Cannon M, Stevenson J, Stahl K, et al. DGIdb 5.0: rebuilding the drug-gene interaction database for precision medicine and drug discovery platforms. *Nucleic Acids Res*. 2024;52(D1):D1227-D1235.
18. Szklarczyk D, Gable AL, Lyon D, et al. STRING v11: protein-protein association networks with increased coverage, supporting functional discovery in genome-wide experimental datasets. *Nucleic Acids Res*. 2019;47(D1):D607-D613.
19. Xu L, Su Y. Genetic pathogenesis of immunoglobulin light chain amyloidosis: basic characteristics and clinical applications. *Exp Hematol Oncol*. 2021;10(1):43.
20. Grabski IN, Street K, Irizarry RA. Significance analysis for clustering with single-cell RNA-sequencing data. *Nat Methods*. 2023;20(8):1196-1202.
21. Chandraditya Chakraborty YX, Yao Yao, Eugenio Morelli, Anil Aktas-Samur, Mehmet Kemal Samur, Mariateresa Fulciniti, Nikhil C. Munshi, Kenneth Anderson, Chandraditya Chakraborty. Activation of the ERK Pathway Drives Acquired Resistance to Venetoclax in MM Cell Models. *Blood*. 2020;Volume 136(Supplement 1):21-22.
22. He H, Lu J, Qiang W, Liu J, Liang A, Du J. The Landscape of Cytogenetic Aberrations in Light-Chain Amyloidosis with or without Coexistent Multiple Myeloma. *J Clin Med*. 2023;12(4).
23. Madan S, Dispenzieri A, Lacy MQ, et al. Clinical features and treatment response of light chain (AL) amyloidosis diagnosed in patients with previous diagnosis of multiple myeloma. *Mayo Clin Proc*. 2010;85(3):232-238.
24. Rajkumar SV, Gertz MA, Kyle RA. Primary systemic amyloidosis with delayed progression to multiple myeloma. *Cancer*. 1998;82(8):1501-1505.
25. Bochtler T, Hegenbart U, Kunz C, et al. Gain of chromosome 1q21 is an independent adverse prognostic factor in light chain amyloidosis patients treated with melphalan/dexamethasone. *Amyloid*. 2014;21(1):9-17.
26. Szalat RE, Talluri S, Royer CM, et al. Composition and Dynamic Evolution of the Bone Marrow Microenvironment in AL Amyloidosis during Daratumumab Based Therapy. *Blood*. 2023;142.
27. Tormoen GW, Crittenden MR, Gough MJ. Role of the immunosuppressive microenvironment in immunotherapy. *Adv Radiat Oncol*. 2018;3(4):520-526.
28. Giannotta C, Autino F, Massaia M. The immune suppressive tumor microenvironment in multiple myeloma: The contribution of myeloid-derived suppressor cells. *Front Immunol*. 2022;13:1102471.

29. Wang Y, Xu L, Liu Y, et al. Transcriptional heterogeneity of clonal plasma cells and immune evasion in immunoglobulin light chain amyloidosis. *Int J Hematol*. 2021;113(2):231-242.
30. Liu R, Gao Q, Foltz SM, et al. Co-evolution of tumor and immune cells during progression of multiple myeloma. *Nat Commun*. 2021;12(1):2559.
31. Bruns I, Cadeddu RP, Brueckmann I, et al. Multiple myeloma-related deregulation of bone marrow-derived CD34(+) hematopoietic stem and progenitor cells. *Blood*. 2012;120(13):2620-2630.
32. Hoelzinger DB, Quinton SJ, Walters DK, et al. Extracellular vesicle proteomic analysis leads to the discovery of HDGF as a new factor in multiple myeloma biology. *Blood Adv*. 2022;6(11):3458-3471.
33. Shi JL, Fu L, Ang Q, Wang GJ, Zhu J, Wang WD. Overexpression of ATP1B1 predicts an adverse prognosis in cytogenetically normal acute myeloid leukemia. *Oncotarget*. 2016;7(3):2585-2595.
34. Bernard BJ, Nigam N, Burkitt K, Saloura V. SMYD3: a regulator of epigenetic and signaling pathways in cancer. *Clin Epigenetics*. 2021;13(1):45.
35. Qian T, Cui L, Liu Y, et al. High expression of chaperonin-containing TCP1 subunit 3 may induce dismal prognosis in multiple myeloma. *Pharmacogenomics J*. 2020;20(4):563-573.
36. Luo SQ, Xiong DH, Li J, et al. C1orf35 contributes to tumorigenesis by activating c-MYC transcription in multiple myeloma. *Oncogene*. 2020;39(16):3354-3366.
37. Feng D, Wang Z, Cao S, Xu H, Li S. Identification of lipid metabolism-related gene signature in the bone marrow microenvironment of multiple myelomas through deep analysis of transcriptomic data. *Clin Exp Med*. 2024;24(1):136.
38. Song H, Liu H, Wang X, et al. Death-associated protein 3 in cancer-discrepant roles of DAP3 in tumours and molecular mechanisms. *Front Oncol*. 2023;13:1323751.
39. Garcia JB, Storti P, Iannozzi NT, et al. Identification of PSMB4 and PSMD4 as novel target genes correlated with 1q21 amplification in patients with smoldering myeloma and multiple myeloma. *Haematologica*. 2024;109(2):627-631.
40. Xiang J, Chen X, Chen M, Hou J. Increased Expression of SETDB1 Predicts Poor Prognosis in Multiple Myeloma. *Biomed Res Int*. 2022;2022:3307873.
41. Xu JH, Guan YJ, Zhang YC, et al. ADAM15 correlates with prognosis, immune infiltration and apoptosis in hepatocellular carcinoma. *Aging (Albany NY)*. 2021;13(16):20395-20417.
42. Sklavenitis-Pistofidis R, Lightbody ED, Reidy M, et al. Large-scale dependency and drug screens characterize the therapeutic vulnerabilities of Multiple Myeloma with 1q. *Blood*. 2025.
43. Fraser C, Presser A, Sanchorawala V, Sarosiek S, Sarosiek K. Clonal plasma cells in AL amyloidosis are dependent on pro-survival BCL-2 family proteins and sensitive to BH3 mimetics 2019.
44. Du T, Song Y, Ray A, et al. Ubiquitin receptor PSMD4/Rpn10 is a novel therapeutic target in multiple myeloma. *Blood*. 2023;141(21):2599-2614.

FIGURE LEGENDS

Figure 1. Overview of study design, cytogenetics, and single-cell analysis. (A) A flowchart illustrating the steps of the study design, which includes sample collection, single-cell RNA sequencing, and subsequent analysis. The figure was created on BioRender.com. (B) The frequency of the most common cytogenetic aberrations (≥4 samples) identified through fluorescent in situ hybridization (FISH) in the AL and AL_MM samples. (C) UMAP projection of aggregated cells (n = 151,164) from 21 patient samples, with each dot representing the transcriptome of an individual cell and a color code indicating distinct clusters. (D) A heatmap summarizing the clinical data of the study cohort (n = 21), which includes diagnosis, median survival (in days), light chain, gender, age at diagnosis, and cytogenetic aberrations. The bottom heatmap displays the percentage of different predicted cell-type populations in the 21 samples.

Figure 2. Plasma cell clusters reveal transcriptional heterogeneity and shared pathways across patient samples. (A) UMAP visualization of six plasma cell clusters, with each dot representing an individual plasma cell. (B) The composition of plasma cells within each plasma cell cluster across the 21 patient samples in the cohort. (C) A heatmap displaying the top 10 differentially expressed genes for each plasma cell cluster (n = 6), where each column corresponds to a plasma cell and each row represents a gene; the top bar indicates the different plasma cell clusters, each marked in distinct colors. (D) Pathway enrichment analysis of plasma cell clusters, highlighting the similarities and differences among different plasma cell clusters.

Figure 3: Distinct changes in cell-type proportion and gene expression in AL_MM_P15 from diagnosis to relapse. (A) Comparison of the percentage of cell types in the paired AL_MM_P15 at both the diagnosis and relapse stages. (B) UMAP visualization of plasma cells from AL_MM at the diagnosis and relapse stages. (C) Boxplot illustrating the differentially expressed genes in plasma cells at the diagnosis and relapse stages for patient AL_MM_P15. (D) Depiction of cell types that show significantly different proportions in AL versus AL_MM samples. (E) Proportion of plasma cells from AL and AL_MM samples for each plasma cell cluster.

Figure 4: Differential gene expression, gene interaction networks, and pathway enrichment differences in AL and AL with co-occurring plasma cells. (A) A heatmap illustrating the differentially regulated genes located on chromosome 1 in AL and AL_MM samples. (B) Boxplots display the expression levels of these differentially regulated genes in the plasma cell population, with each dot representing an individual plasma cell. (C) Relative pathway enrichment analysis of plasma cell populations in AL and AL_MM samples conducted using Single Cell Pathway Analysis (SCPA).

Figure 5: InferCNV analysis reveals differences in chromosomal alterations in plasma cells of AL and AL with co-occurring MM. (A) The heatmap on the left displays the cytogenetic abnormalities identified using the fluorescent in situ hybridization (FISH) technique, while the heatmap on the right illustrates the estimation of copy number variants in plasma cells from AL and AL_MM samples using inferCNV. (B) Boxplots displaying the chromosomal cytobands where amplifications or deletions were significantly different ($p<0.05$) between the AL and AL_MM groups.

Table1: Patient characteristics.

Patient ID	Diagnosis	Disease status	Age at the time of diagnosis	Gender	Light chain type mm	FISH Findings	Median Survival time (Months)
AL_P01	AL	Diagnosis	61-65	Female	lambda	t(11;14), trisomy 11, other abnormality, monosomy 12	84.76
AL_P02	AL	Diagnosis	61-65	Male	lambda	del(13q), other abnormality, del(14q32)	63.21
AL_P03	AL	Diagnosis	71-75	Male	lambda	IgH deletion	60.38
AL_MM_P04	AL, sMM	Diagnosis	51-55	Female	kappa	t(14;20), del(13q)/-13	176.77
AL_P05	AL	Diagnosis	81-85	Male	-	-	25.85
AL_P06	AL	Diagnosis	61-65	Female	-	Monosomy 13, del(14q32), structurally abnormal chromosome 1	1.28
AL_MM_P07	AL, MM	Diagnosis	66-70	Female	lambda	-	6.44
AL_MM_P08	AL, sMM	Diagnosis	61-65	Female	lambda	1q gain, other abnormality, 11	96.75
AL_P09	AL	Diagnosis	71-75	Female	lambda	-	40.37
AL_MM_P10	AL, MM	Diagnosis	61-65	Male	lambda	del(13q), del(17p13), t(11;14), 1q gain, other abnormality, del(11q)	14.75
AL_P11	AL	Diagnosis	51-55	Male	-	t(11;14), monosomy 13	25.92
AL_MM_P12	AL, MM	Diagnosis	46-50	Female	kappa	del(13q), 1q gain, other abnormality, IgH deletion	25.10
AL_P13	AL	Diagnosis	66-70	Male	-	t(11;14)	8.31
AL_MM_P14	AL, MGUS	Diagnosis	71-75	Male	lambda	1q gain, other abnormality, IgH (14q32) translocation	22.70
AL_MM_P15_D	AL, sMM	Diagnosis	66-70	Male	lambda	1q gain	59.30
AL_MM_P15_R	AL, sMM	Relapse	66-70	Male	lambda	1q gain	
AL_P16	AL	Diagnosis	66-70	Male	-	-	73.29
AL_P17	AL	Diagnosis	76-80	Male	lambda	t(11;14), other abnormality, monosomy 12	54.66
AL_MM_P18	AL, sMM	Diagnosis	66-70	Male	lambda	1p32/p36 loss, trisomy 11	52.69
AL_P19	AL	Diagnosis	55-60	Female	lambda	t(6;14), trisomy 11	53.61
AL_P20	AL	Diagnosis	61-65	Male	lambda	Trisomy 11, monosomy 13	5.03

*AL= Amyloidosis; MM= Multiple myeloma; sMM= smoldering multiple myeloma; MGUS= Monoclonal gammopathy of unknown significance.

Figure 1. Clinical and cytogenetic characterization of AL amyloidosis and co-occurring multiple myeloma/MGUS.

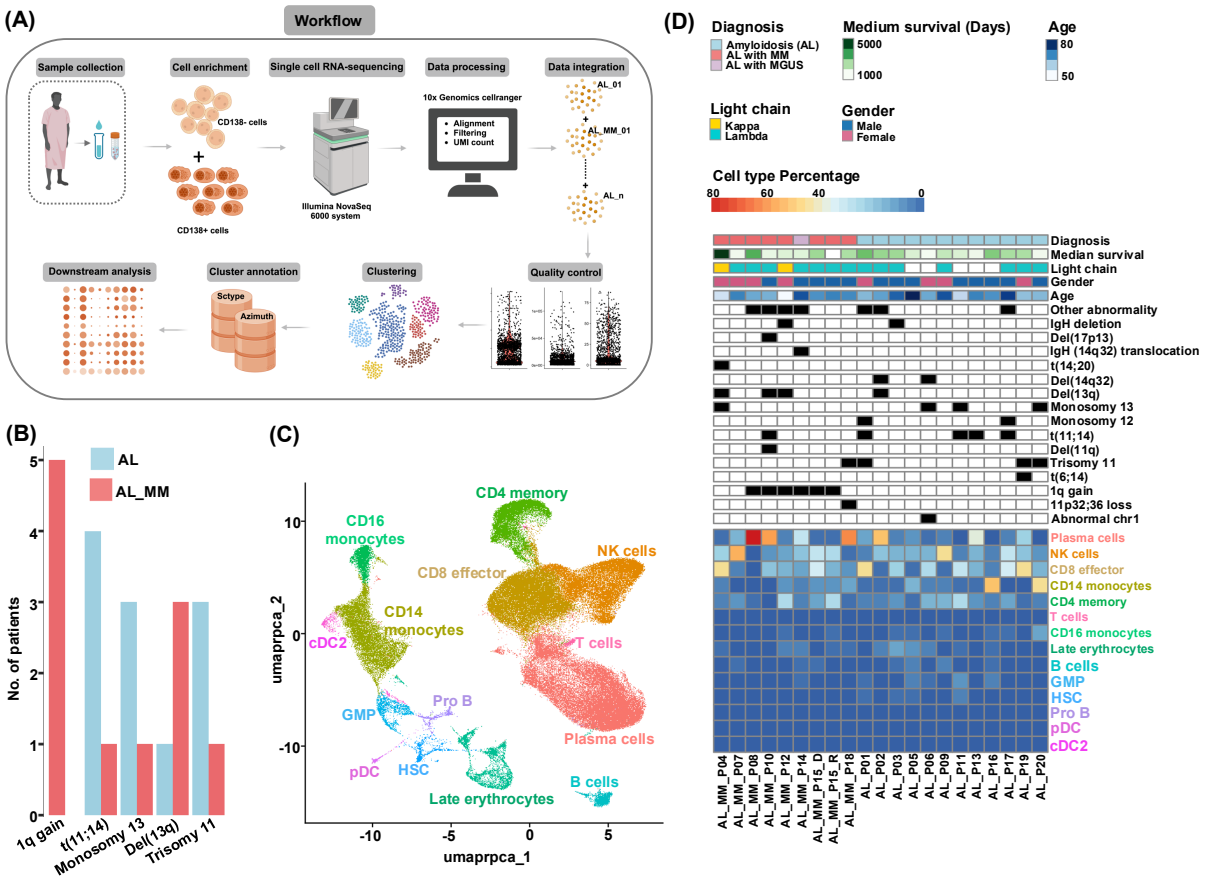

Figure 2. Plasma cell clusters reveal transcriptional heterogeneity and shared pathways across patient samples

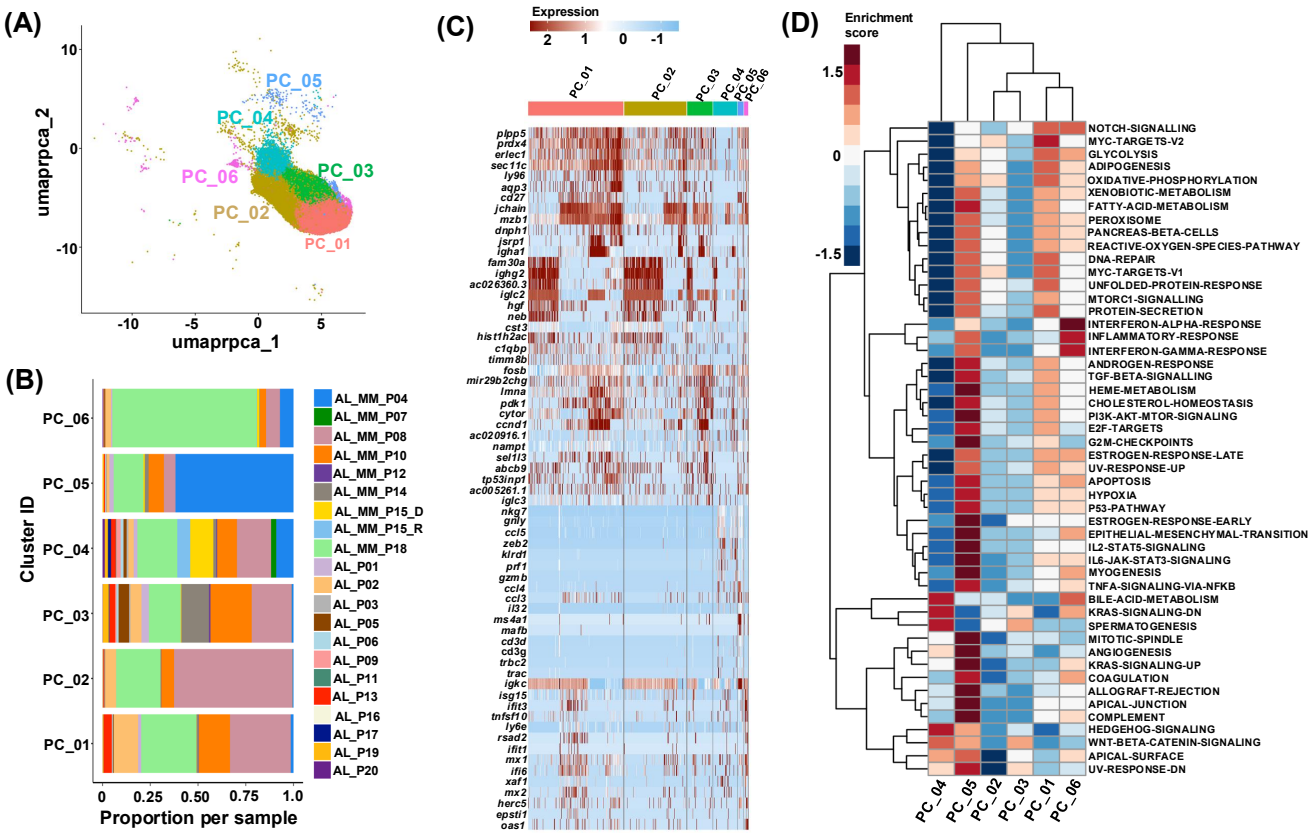

Figure 3: Distinct changes in cell-type proportion and gene expression in AL_MM_P15: Diagnosis vs. Relapse

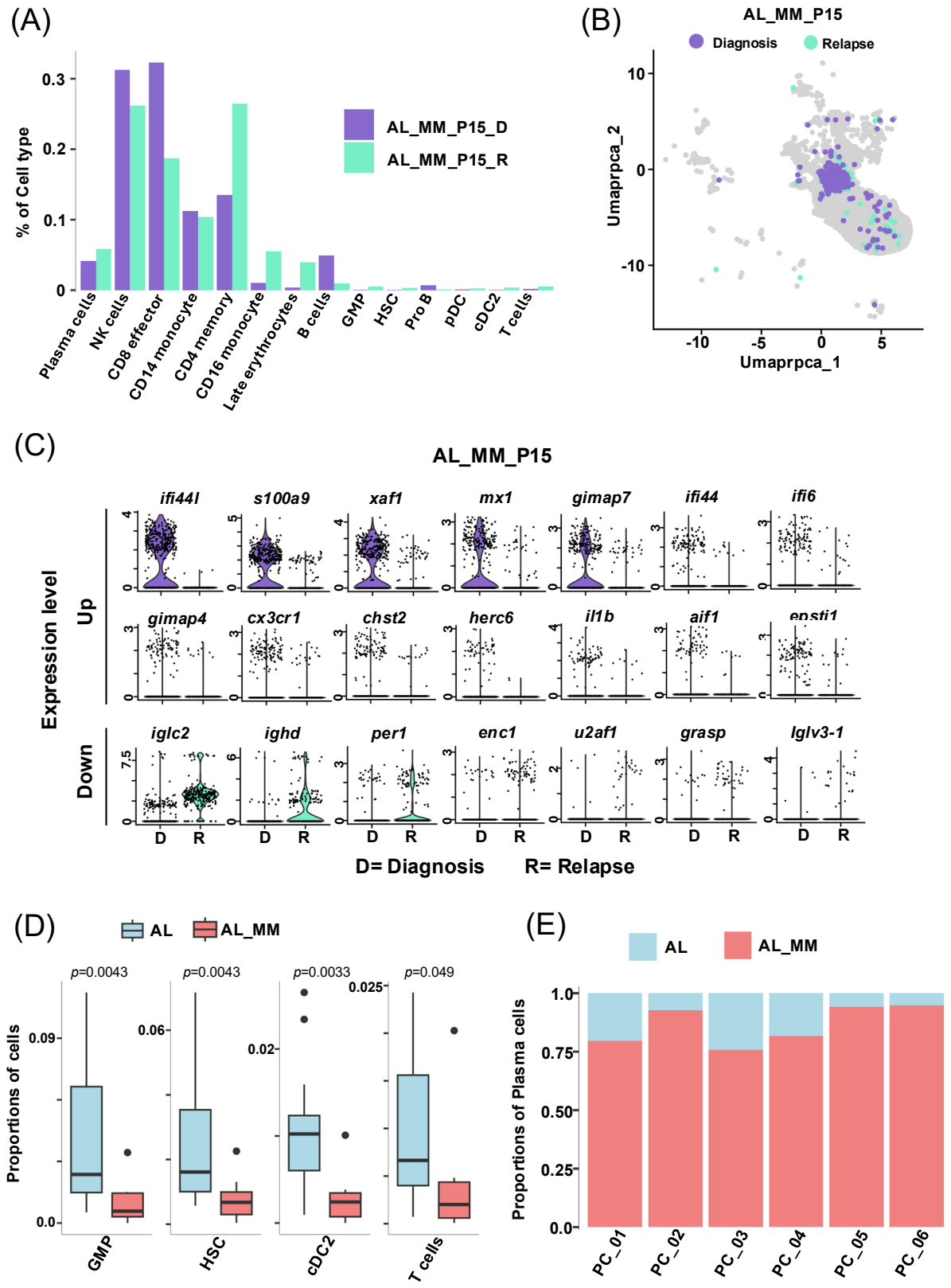

Figure 4: Differential gene expression, gene interaction networks, and pathway enrichment differences in AL and AL_MM plasma cells

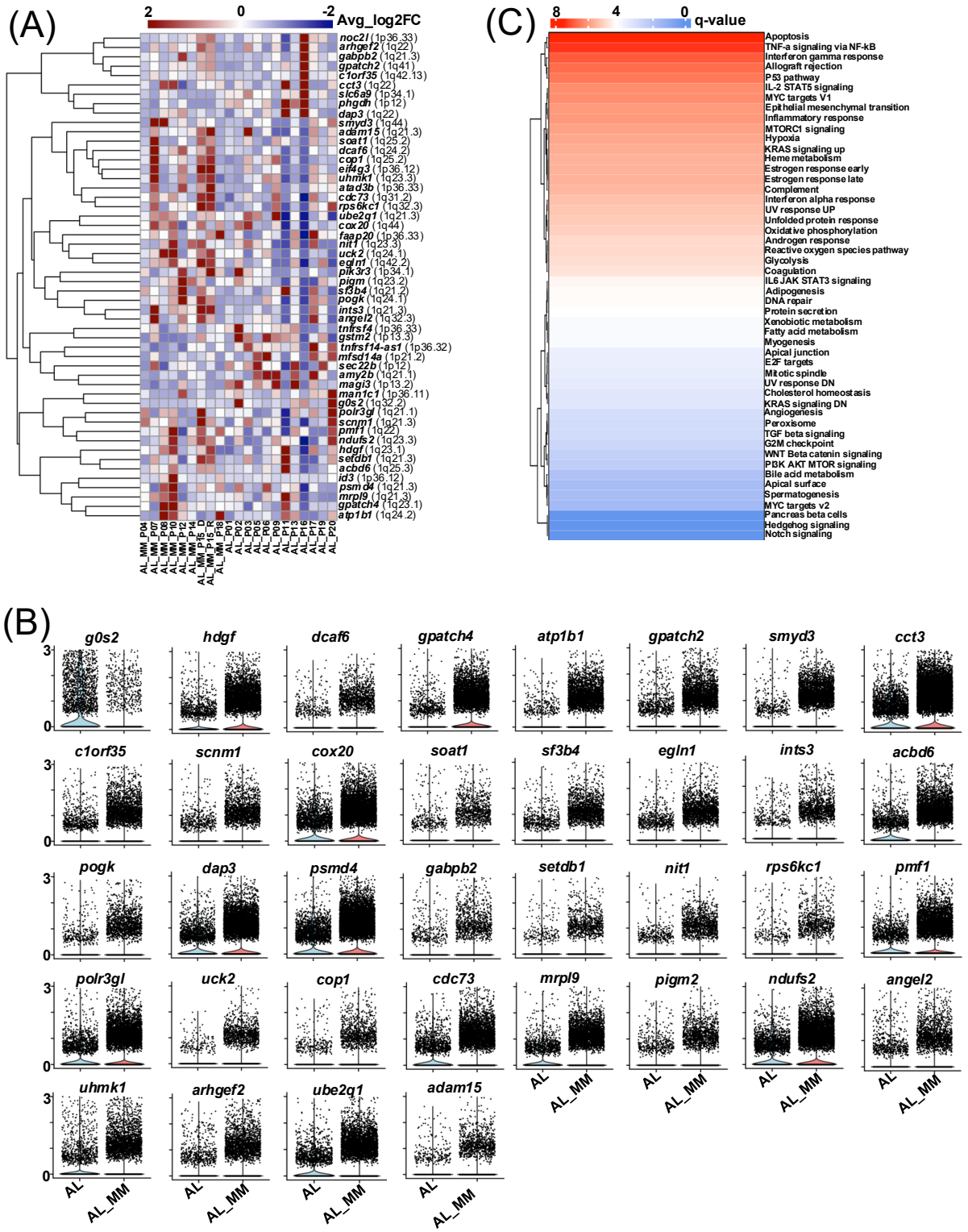
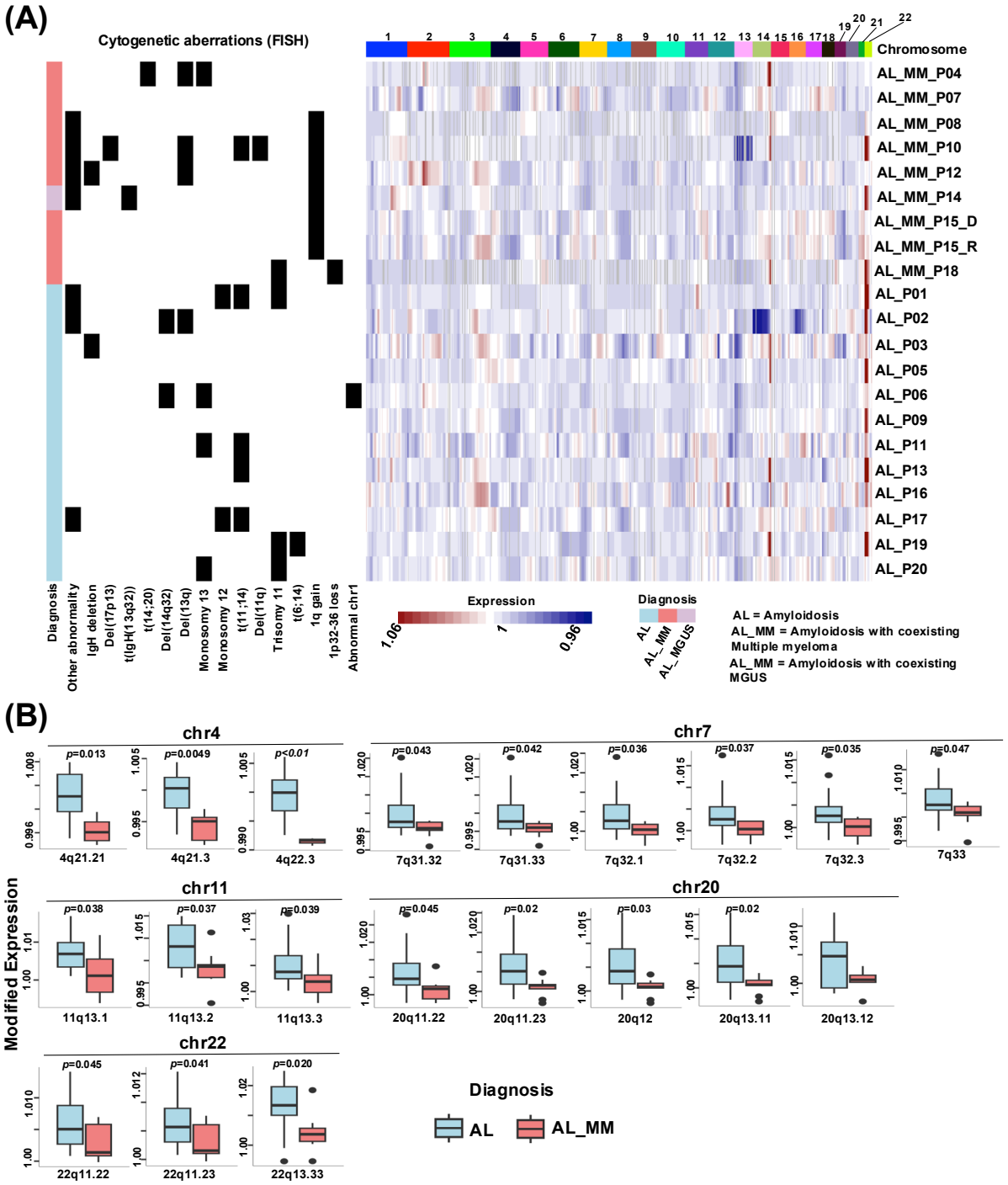
Figure 5: InferCNV analysis reveals differences in chromosomal alterations in AL and AL_MM plasma cells.